

Camera Pose Correction in SLAM Based on Bias Values of Map Points

Zhaobing Kang, Wei Zou and Zheng Zhu

Abstract—Accurate camera pose estimation result is essential for visual SLAM (VSLAM). This paper presents a novel pose correction method to improve the accuracy of the VSLAM system. Firstly, the relationship between the camera pose estimation error and bias values of map points is derived based on the optimized function in VSLAM. Secondly, the bias value of the map point is calculated by a statistical method. Finally, the camera pose estimation error is compensated according to the first derived relationship. After the pose correction, procedures of the original system, such as the bundle adjustment (BA) optimization, can be executed as before. Compared with existing methods, our algorithm is compact and effective and can be easily generalized to different VSLAM systems. Additionally, the robustness to system noise of our method is better than feature selection methods, due to all original system information is preserved in our algorithm while only a subset is employed in the latter. Experimental results on benchmark datasets show that our approach leads to considerable improvements over state-of-the-art algorithms for absolute pose estimation.

I. INTRODUCTION

VSLAM can estimate the camera trajectory and reconstruct environment, therefore, it is very important on many occasions, such as mobile robots navigation and augmented reality (AR). To improve the accuracy, parallelism [1] and orthogonality [4] of lines or planes are utilized. However, since no prior structural information is acquired when exploring new environments, they cannot be used. Unlike the above methods, the optimization-based methods [5], [21] or the matrix-theory-based approach [13] are not limited by the environment. But most pipelines of them are complex and difficult to combine with different SLAM systems. Multi-sensor fusion can compensate the drawbacks of each other, therefore, the IMU is widely used in VSLAM to improve the system robustness [20], [24], [25]. However, accurate IMU bias estimation is difficult, and large estimation error may affect the localization performance of the SLAM system.

This paper presents a novel pose correction method, which is compact and effective and reserves all original system information. The most related work to this paper is [14], where the map points with small bias value are chosen to estimate the camera pose while the other map points are abandoned. Different from choosing a subset of map points to reduce the estimation error in [14], our method compensates the pose estimation error based on the bias values of all map points.

Our algorithm has two advantages compared with existing methods. The first advantage is our method is compact and effective and easy to integrate into different SLAM systems. The second is the robustness of our method is better than feature selection methods, such as [14]. Since only a subset

of features is chosen in feature selection methods, they are more sensitive to system noise, which is demonstrated by the experimental results.

II. RELATED WORKS

Structural regularity based methods: A monocular SLAM system, which leverages structural regularity in Manhattan world and contains three optimization strategies is proposed in [1]. However, to reduce the estimation error of the rotation motion, multiple orthogonal planes must be visible throughout the entire motion estimation process. Unlike only using planes in [1], the rotation motion is estimated by joint lines and planes in [2]. Once the rotation is found, the translational motion can be recovered by minimizing the de-rotated reprojection error. In [3], the accuracy of BA optimization is enhanced by incorporating feature scale constraints into it. Structural constraints between nearby planes (e.g. right angle) are added in the SLAM system to further recover the drift and distortion in [4]. Since the structural regularity does not exist in all environments, the application scope of this category is limited.

Optimization-based methods and matrix-theory-based methods: A new initialization method for the orientations of the pose graph optimization problem is proposed in [5]. In this method, the orientation values are calculated by an iterative approach, and the relative orientation mismatches of the cost function are approximated by a quadratic cost function. In [6], the photometric and the depth error over all pixels are employed to reduce the estimation error in the RGB-D system. However, this method is time-consuming and difficult to achieve real-time performance. Different from using all pixel depth information in [6], a monocular camera combined with sparse depth information from LiDAR is employed in [7], and three optimization strategies are carefully designed considering both accuracy and time-consuming. Similar to [6] and [7], a new approach, which utilizes dense fusion of several stereo depths in the locality establishes a locally dense and globally sparse map. Rao-Blacwellized particle filter (RBPF) method is employed in [8] and [9]. The difference between them is [8] presents a new RBPF method while drawbacks of the RBPF are overcome in [9] by scaled unscented transformation. How to obtain accurate map in the large or scale uncertain environments is studied in [10]–[12]. To get a good accuracy without sacrificing speed, new matrix decompose methods are proposed in [13] and [15]. Different from the above methods, where all system information is employed, a good feature selection algorithm is introduced in [14]. By selecting the map

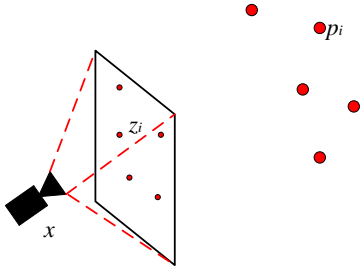


Fig. 1. The commonly used SLAM system. In this figure, the map point p_i is projected to the image point z_i at the camera pose x .

points which have smaller error, it can reach a balance between the error expectation and the covariance. Most pipelines of them are complex, therefore, it is difficult to integrate them into different SLAM systems.

Methods of integration with IMU: In [16], four cameras and an IMU are tightly fused in a Micro Aerial Vehicle (MAV). A new approach tightly combines visual measurements with IMU measurements is proposed in [17]. The novelty lies in that the IMU error term is integrated with the landmark reprojection error in a fully probabilistic manner. In [18], IMU information is employed in the ORB-SLAM [19] to solve the scale problem of a monocular system. The performance of the SLAM system is easily affected by the bias estimation results and IMU noise.

The main contributions of this paper can be summarized as follows. (i) A new camera pose correction method is proposed. (ii) A bias calculating method used for the map point is integrated into our framework. Thanks to this method, our system can operate in real-time. (iii) Experimental results demonstrate that our method outperforms the state-of-the-art SLAM system.

III. RELATIONSHIP BETWEEN POSE ESTIMATION ERROR AND MAP POINT BIAS

The commonly used SLAM system is shown in Fig. 1. In this system, the main object is to estimate the camera pose x and the map point p_i by minimizing the errors between the observation values and the estimation values, which can be written as

$$\arg \min_{x, p_i} \frac{1}{2} \sum_{i=1}^n \|h(x, p_i) - z_i\|^2 \quad (1)$$

where n represents the number of matched image feature point z_i at the camera pose x , and $h(x, p_i)$ represents the camera projection model. To simplify the description, for the symbols whose dimension can be easily determined, the subscripts of them are omitted. This problem can be solved by the Gaussian-Newton method or the Levenburg-Marquadt (LM) method. Since $h(x, p_i)$ is a nonlinear function, it must be linearized to fit for these optimization methods. The first-

order approximation to $h(x, p_i)$ about initial guess $x^{(s)}$ can be written as

$$h(x, p_i) = h(x^{(s)}, p_i) + \mathbf{H}_x(x - x^{(s)}) \quad (2)$$

where \mathbf{H}_x is the Jacobian matrix about x . Similar to (2), the first-order approximation to $h(x^{(s)}, p_i)$ about initial guess $p_i^{(s)}$ is

$$h(x^{(s)}, p_i) = h(x^{(s)}, p_i^{(s)}) + \mathbf{H}_{p_i}(p_i - p_i^{(s)}) \quad (3)$$

where \mathbf{H}_{p_i} is the Jacobian matrix about p_i .

According to the Gaussian-Newton method, (1) and (2), the pose update can be written as

$$x^{(s+1)} = x^{(s)} - \mathbf{H}_x^+ (h(x^{(s)}, p_i) - z_i) \quad (4)$$

where \mathbf{H}_x^+ is the pseudo-inverse of \mathbf{H}_x . Substituting (3) into (4), the pose estimation error is

$$\epsilon_x = -\mathbf{H}_x^+ (\mathbf{H}_{p_i} \epsilon_{p_i} + \epsilon_{z_i}) \quad (5)$$

where $\epsilon_x = x^{(s+1)} - x^{(s)}$ represents the pose estimation error, $\epsilon_{z_i} = h(x^{(s)}, p_i^{(s)}) - z_i$ represents the observation error, and $\epsilon_{p_i} = p_i - p_i^{(s)}$ represents the map point bias.

Suppose the image observation error subjects to the zero-mean Gaussian distribution, i.e. $\epsilon_{z_i} \sim N(\mathbf{0}, \Sigma_{z_i})$, and the error of the map point subjects to non-zero-mean Gaussian distribution, i.e. biased distribution $\epsilon_{p_i} \sim N(\mu_{p_i}, \Sigma_{p_i})$. This assumption is reasonable, because the bias of the map point can be introduced by the BA optimization or the image measurement error. According to this assumption, the expectation of the camera pose estimation error is

$$E[\epsilon_x] = -\mathbf{H}_x^+ \mathbf{H}_{p_i} \mathbf{1} \mu_p. \quad (6)$$

where

$$\mathbf{1} = \begin{bmatrix} 1 & 1 & 1 & 0 & 0 & 0 & \dots & 0 & 0 & 0 \\ 0 & 0 & 0 & 1 & 1 & 1 & \dots & 0 & 0 & 0 \\ \vdots & \vdots & \vdots & \vdots & \vdots & \vdots & \vdots & \vdots & \vdots & \vdots \\ 0 & 0 & 0 & 0 & 0 & 0 & \dots & 1 & 1 & 1 \end{bmatrix}_{3n \times 3n}. \quad (7)$$

It is obvious that the pose estimation error can be reduced if the bias value of the map point is known. However, getting accurate bias value is difficult due to system errors. In this paper, a bias calculating expression proposed in [29] is employed, which will be introduced in the next section.

IV. CAMERA POSE CORRECTION

A. Bias Calculation

The basic idea of the bias calculating method is introduced in this subsection, and more details can be available in [29]. Let $\mathbf{V} = [v_x, v_y, v_z]^T$ and $\mathbf{\Omega} = [\omega_x, \omega_y, \omega_z]^T$ respectively represent the translation vector and the rotation vector of the camera. According to the optical flow, 3D camera motion and

TABLE I
THE SYMBOL MEANINGS USED IN THE BIAS EXPRESSION.

Symbol	Meaning
(x_i, y_i)	the image coordinates of the point z_i
(x_f, y_f)	the focus of expansion (FOE), equals to $(V_x/V_z, V_y/V_z)$
$z(x_i, y_i)$	the depth of the point z_i
\mathbf{d}	$(d(x_1, y_1), \dots, d(x_N, y_N))^T$
\mathbf{u}	$(p(x_1, y_1), q(x_1, y_1), \dots, p(x_N, y_N), q(x_N, y_N))^T$
\mathbf{r}_i	$(x_i y_i, -(1+x_i^2), y_i)^T$
\mathbf{s}_i	$(1+y_i^2, -x_i y_i, -x_i)^T$
$\mathbf{\Omega}$	$(\omega_x, \omega_y, \omega_z)^T$
\mathbf{Q}	$[\mathbf{r}_1, \mathbf{s}_1, \dots, \mathbf{r}_N, \mathbf{s}_N]^T$
\mathbf{P}	diagonal matrix $\text{diag} \begin{bmatrix} x_i - x_f \\ y_i - y_f \end{bmatrix}_{2N \times N, i=1, \dots, N}$
\mathbf{B}	$\begin{bmatrix} \mathbf{P} & \mathbf{Q} \\ \mathbf{d} & \mathbf{\Omega} \end{bmatrix}$
\mathbf{z}	$\begin{bmatrix} \mathbf{d} \\ \mathbf{\Omega} \end{bmatrix}$

scene depth, the velocity fields of the image point z_i can be expressed as

$$\begin{aligned}
 p(x_i, y_i) &= (x_i - f x_f) d(x_i, y_i) + \frac{1}{f} x_i y_i \omega_x \\
 &\quad - \left(f + \frac{1}{f} x_i^2 \right) \omega_y + y_i \omega_z \\
 q(x_i, y_i) &= (y_i - f y_f) d(x_i, y_i) - \frac{1}{f} x_i y_i \omega_y \\
 &\quad + \left(f + \frac{1}{f} y_i^2 \right) \omega_x - x_i \omega_z
 \end{aligned} \tag{8}$$

where $p(x_i, y_i)$ and $q(x_i, y_i)$ are the horizontal and vertical velocity fields, $d(x_i, y_i) = v_z/z(x_i, y_i)$ is the scaled inverse scene depth, and the meanings of the other parameters are listed in Table I. For N matched feature points in two consecutive frames, normalizing linear distances with respect to the focal length, (8) can be written as a matrix form

$$\mathbf{u} = \mathbf{P}\mathbf{d} + \mathbf{Q}\mathbf{\Omega} = [\mathbf{P} \ \mathbf{Q}] \begin{bmatrix} \mathbf{d} \\ \mathbf{\Omega} \end{bmatrix} \triangleq \mathbf{B}\mathbf{z} \tag{9}$$

where the meanings of symbols are shown in Table I. The aim is calculating \mathbf{z} from \mathbf{u} . For VSLAM, since the camera motions corresponding to these two frames are known, $\mathbf{\Omega}$ is known. (9) can be rewritten as

$$\mathbf{b} = \mathbf{A}\mathbf{d} \tag{10}$$

where

$$\begin{aligned}
 \mathbf{A} &\triangleq \mathbf{P} \\
 \mathbf{b} &\triangleq \begin{bmatrix} p(x_1, y_1) - \mathbf{r}_1^T \mathbf{\Omega}, q(x_1, y_1) - \mathbf{s}_1^T \mathbf{\Omega}, \dots, \\ p(x_N, y_N) - \mathbf{r}_N^T \mathbf{\Omega}, q(x_N, y_N) - \mathbf{s}_N^T \mathbf{\Omega} \end{bmatrix},
 \end{aligned}$$

where the meanings of \mathbf{r}_i and \mathbf{s}_i are listed in Table I. The least square solution of (10) is

$$\hat{\mathbf{d}} = (\mathbf{A}^T \mathbf{A})^{-1} \mathbf{A}^T \mathbf{b} \tag{11}$$

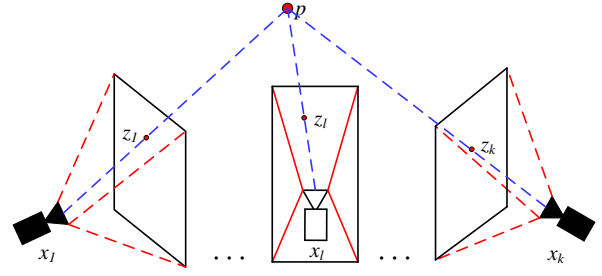


Fig. 2. Recover map points using k frames in VSLAM. In this figure, the map point \mathbf{p} is projected to the image point \mathbf{z} . If \mathbf{p} can be observed by k images, then it can be jointly recovered by these k images.

To simplify the description of the bias expression, let

$$\begin{aligned}
 \mathbf{M} &\triangleq \mathbf{A}^T \mathbf{A} = \text{diag} \left[(x_i - x_f)^2 + (y_i - y_f)^2 \right]_{N \times N} \\
 &= \text{diag} [m_{ii}]_{i=1 \dots N}
 \end{aligned}$$

$$\begin{aligned}
 \mathbf{V} &\triangleq \mathbf{A}^T \mathbf{b} = \text{diag} [(x_i - x_f) v_{pi} + (y_i - y_f) v_{qi}]^T \\
 &\triangleq [v_1 \dots v_N]^T
 \end{aligned}$$

where $v_{pi} = p(x_i, y_i) - \mathbf{r}_i^T \mathbf{\Omega}$, $v_{qi} = q(x_i, y_i) - \mathbf{s}_i^T \mathbf{\Omega}$ and $\text{diag}[\]$ represents the diagonal matrix.

According to [29], the bias of the inverse depth estimation of the i^{th} feature point is

$$\begin{aligned}
 \mu(\hat{\mathbf{d}}_i) &= \frac{2\sigma_i^2 v_i}{m_{ii}^2} \\
 &\quad + \frac{2\sigma_i^2}{m_{ii}^2} \left[(x_i - x_f)^2 \mathbf{r}_{ix}^T + (y_i - y_f)^2 \mathbf{s}_{iy}^T \right] \mathbf{\Omega} \\
 &\quad + \frac{2\sigma_i^2}{m_{ii}^2} \left[(x_i - x_f)(y_i - y_f) (\mathbf{r}_{iy}^T + \mathbf{s}_{ix}^T) \right] \mathbf{\Omega} \\
 &\quad + \frac{\sigma_i^2}{m_{ii}^2} \left[(x_i - x_f) \omega_y - (y_i - y_f) \omega_x - (\mathbf{r}_{ix}^T + \mathbf{s}_{iy}^T) \mathbf{\Omega} \right]
 \end{aligned} \tag{12}$$

where σ_i^2 is the variance in the image coordinate measurements, \mathbf{r}_{ix} and \mathbf{s}_{ix} is the derivative of \mathbf{r}_i and \mathbf{s}_i with respect to x , and \mathbf{r}_{iy} and \mathbf{s}_{iy} have similar meanings.

Since the depth result is easily affected by the noise for two-frame reconstruction, L two-frame reconstruction results are employed to reduce the depth error, where the depth result and the bias are

$$\hat{\mathbf{d}} = \frac{1}{L} \sum_{j=1}^L \hat{\mathbf{d}}^j \tag{13}$$

$$\boldsymbol{\mu}(\hat{\mathbf{d}}) = \frac{1}{L} \sum_{j=1}^L \boldsymbol{\mu}(\hat{\mathbf{d}}^j) \tag{14}$$

For the biased estimation, $E[\hat{\mathbf{d}}] = \bar{\mathbf{d}} + \boldsymbol{\mu}(\hat{\mathbf{d}})$, where $\bar{\mathbf{d}}$ is the truth-value. If $\hat{\mathbf{d}}_c = \hat{\mathbf{d}} - \boldsymbol{\mu}(\hat{\mathbf{d}})$, then $E[\hat{\mathbf{d}}_c] = E[\hat{\mathbf{d}}] - \boldsymbol{\mu}(\hat{\mathbf{d}}) = \bar{\mathbf{d}}$. $\hat{\mathbf{d}}_c$ is an unbiased estimation.

In VSLAM, map points can be observed by multi-frames, which is shown in Fig. 2. Therefore, map points are jointly

recovered by these frames, and $\mu(\hat{\mathbf{d}})$ may not be the bias value of map points due to it is derived based on two-frame. To solve this problem, we first reconstruct map points using multi-two-frame, and getting $\hat{\mathbf{d}}$ and $\mu(\hat{\mathbf{h}})$ according to (13) and (14). Then $\hat{\mathbf{d}}_c$ can be obtained. Since $\hat{\mathbf{d}}_c$ is an unbiased estimation, suppose the actual value acquired by multi-frame is $\tilde{\mathbf{d}}$, the bias value of map points is $\mu(\tilde{\mathbf{d}}) = \tilde{\mathbf{d}} - \hat{\mathbf{d}}_c$. According to the bias value $\mu(\tilde{\mathbf{d}})$ and (6), the camera pose estimation error can be corrected.

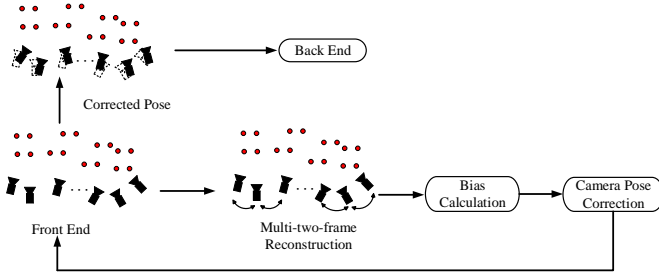


Fig. 3. A block diagram illustrating the full pipeline of our camera pose correction method.

B. Anomaly detection strategy

In practical applications, bias values of some map points may be very large due to mismatching or camera motion error, which can make the system unstable. To avoid this negative effect, we propose a heuristic strategy to determine which map points can be used to compensate the pose estimation error. Since the bias value is negative correlation to the image parallel, the principle of our strategy is choosing map points recovered by large parallels. In this article, our method is combined with the VINS-Mono [20] where the camera motion is detected by the IMU. Therefore, the parallel can be replaced by the camera angular velocity. The strategy is

$$\text{thresh of bias} = \begin{cases} 0.1m & \text{if } \|\omega_{cam}\|_2 \geq 0.5 \\ 0.3m & \text{if } 0.3 \leq \|\omega_{cam}\|_2 < 0.5 \\ 0.5m & \text{if } \|\omega_{cam}\|_2 < 0.3 \end{cases} \quad (15)$$

where $\|\omega_{cam}\|_2$ represents the l_2 -norm of the angular velocity. If the bias value of the map point is larger than the thresh value, the corresponding map point is abandoned to correct the pose error. These thresh values are set based on testing results in different datasets, which makes our algorithm get stable and accurate results.

The full pipeline of our camera pose correction method is shown in Fig. 3. In this figure, the camera pose obtained by the front end is used to calculate the depth and bias of map points according to (11) and (12). To make full use of all frames which observes the same map points, multi-two-frame reconstructions are processed. Based on reconstruction results, bias value is calculated by (13) and (14), and the camera pose error in front end is corrected. Finally the results of the front end are optimized by the back end. Our algorithm

only modifies the results obtained by the front end and is independent of the back end. Therefore, it is easy to integrate into different VO/SLAM systems.

Remark 1: In abstract and Section I, we emphasize that one of characteristics of our method is all original system information is reserved. It is not contradict some map points may be abandoned to correct the pose error, because pose correction is a separate procedure. This means that steps of the original system are not changed, therefore, all system information still can be used after the pose correction.

V. EXPERIMENTS

The effectiveness of our method is verified by integrating it into the VINS-Mono framework. Our algorithm is activated after finishing initialization. The pose error correction is implemented if feature points are successfully tracked and triangulated, and finally BA optimization is executed. The experiments are performed in an Intel Core i7-2670QM computer with 8GB RAM, and we evaluate the accuracy in the EuroC dataset [23]. To make results more reliable, we run five times in each sequence for every compared method and calculate the mean value as their final results.

A. Compared results with VINS-Mono based methods

The accuracy of our method is compared with the original VINS-Mono and the good feature selection method (GF) [14] mentioned at the end of Section I. Based on the published source code of [14], which is realized based on the ORB-SLAM, we combine it with the VINS-Mono and set the number of selected map points in the sliding window to 50. This value is large enough to make the estimation result reach a good balance between the accuracy and confidence. If the number of map points in the sliding window is less than 50, all of them are used in BA optimization to avoid the side effect caused by too little map points. Other parameters in these methods are the same. The translation Root Mean Square Error (RMSE) and the median errors of the keyframe trajectory for each sequence are shown in Table II and Table III, respectively. The first three columns represent the results without loop detection, and the results with loop detection are given in the last three columns.

It can be seen that our method performs best on at least seven of ten sequences no matter in the system with or without loop detection. Especially for the RMSE result with loop detection, the accuracies in nine sequences are largely improved, e.g. $0.12m$ to $0.06m$ in the sequence MH_01_easy and $0.16m$ to $0.088m$ in the sequence V2_02_medium. The difference to the best system on the other sequences is small. For the GF method, due to only a subset of map points is employed in BA optimization, the robustness of the estimation result to the IMU noise is reduced. That is the reason why the performance of VINS-Mono decreases after combined with the GF method. The compared results with the GF algorithm demonstrate the advantage of our method, i.e. robustness to system noise. It guarantees our system can still achieve a good performance in systems contain the IMU or little map points.

TABLE II
THE RMSE ERROR OF CAMERA POSE ESTIMATION RESULTS (UNIT: M).

Sequence	Our method no loop	VINS-Mono no loop	VINS-GF no loop	Our method with loop	VINS-Mono with loop	VINS-GF with loop
MH_01_easy	0.20	0.15	0.24	0.06	0.12	0.22
MH_02_easy	0.15	0.15	0.15	0.07	0.12	0.47
MH_03_medium	0.21	0.22	0.27	0.078	0.13	0.17
MH_04_difficult	0.31	0.32	0.36	0.11	0.18	0.16
MH_05_difficult	0.25	0.30	0.29	0.12	0.21	0.17
V1_01_easy	0.089	0.079	0.095	0.048	0.068	0.070
V1_02_medium	0.09	0.11	0.096	0.050	0.084	0.068
V1_03_difficult	0.15	0.18	0.20	0.212	0.19	0.195
V2_01_easy	0.092	0.080	0.093	0.050	0.081	0.081
V2_02_medium	0.13	0.16	0.13	0.088	0.16	0.18
Average error	0.1671	0.1799	0.1924	0.0886	0.1343	0.1784

TABLE III
THE MEDIAN ERROR OF CAMERA POSE ESTIMATION RESULTS (UNIT: M).

Sequence	Our method no loop	VINS-Mono no loop	VINS-GF no loop	Our method with loop	VINS-Mono with loop	VINS-GF with loop
MH_01_easy	0.16292	0.17504	0.19594	0.05087	0.12	0.15811
MH_02_easy	0.11173	0.08014	0.08317	0.05377	0.06140	0.34695
MH_03_medium	0.18585	0.20008	0.20036	0.05888	0.07544	0.11668
MH_04_difficult	0.35914	0.40284	0.38965	0.10408	0.11880	0.13352
MH_05_difficult	0.25327	0.23488	0.29118	0.10486	0.17543	0.14442
V1_01_easy	0.07016	0.07120	0.07257	0.04345	0.05756	0.06305
V1_02_medium	0.08712	0.09171	0.09319	0.04549	0.05951	0.06257
V1_03_difficult	0.11329	0.16920	0.18705	0.16260	0.16229	0.17792
V2_01_easy	0.06844	0.05234	0.06680	0.04313	0.05099	0.06538
V2_02_medium	0.08515	0.08650	0.08644	0.07149	0.11029	0.12626
Average error	0.14970	0.15639	0.16663	0.06337	0.09917	0.13948

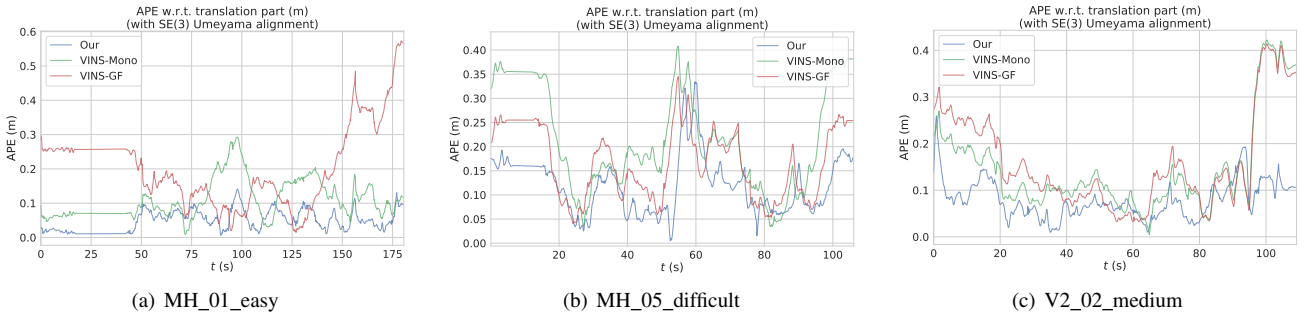


Fig. 4. The curves of absolute pose error (APE) w.r.t. translation part of sequences MH_01_easy, MH_05_difficult and V2_02_medium. The results are acquired in the system with loop detection.

To show the details of pose estimation error, we visualize the absolute pose error (APE) w.r.t. translation part of sequences MH_01_easy, MH_05_difficult and V2_02_medium in Fig. 4 and Fig. 5. According to Fig. 4, it is obvious that our method has the smallest translation error, especially at the beginning and the end of the trajectory. This result shows superiority of our method in suppressing the accumulative error. Fig. 5 shows the box plot of the translation error. In this figure, the dark line represents the mean value of the error, and the height of the box represents the variance. From this figure, the mean value of our method is less than $0.1m$ in sequences MH_01_easy and V2_02_medium and about $0.1m$ in the sequence MH_05_difficult, while the mean value of compared methods are more than $0.1m$ in sequences

MH_01_easy and V2_02_medium and more than $0.15m$ in the sequence MH_05_difficult. Meanwhile, the variance of our method is also the smallest. This result further demonstrates the effectiveness and stability of our method in reducing the pose estimation error.

We also show the trajectory of the sequence MH_01_easy with loop detection in Fig. 6. In this figure, due to the influence of IMU noise, the GF method cannot return to the original point at the end of the trajectory.

B. Compared results with other VIO methods

The accuracy of our method is also compared with another four state-of-the-art visual inertial odometry (VIO) algorithms, R-VIO [24], ROVIO [25], MSCKF [27] and OKVIS [28]. Since loop detection is not available in some of them, only

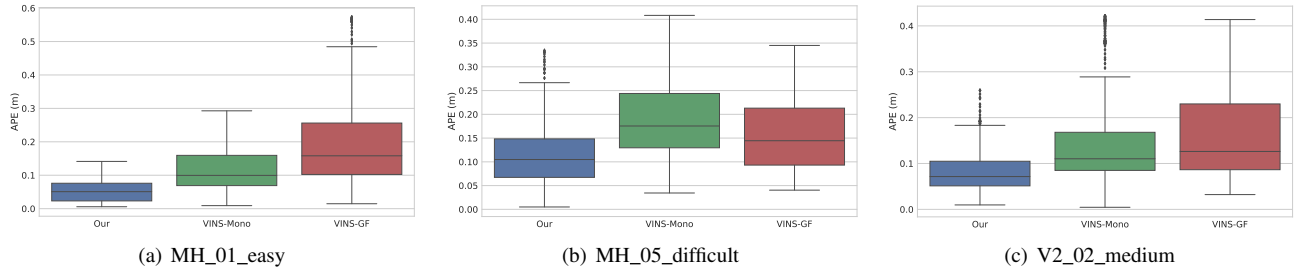


Fig. 5. The box plot of absolute pose error (APE) w.r.t. translation part corresponding to Fig. 4.

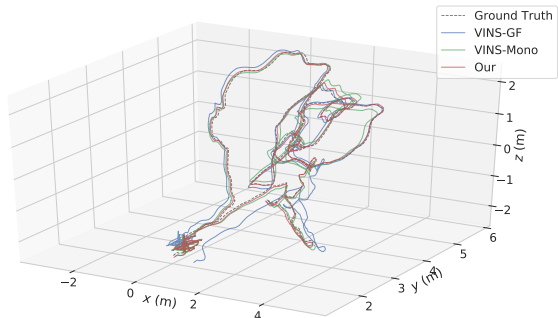


Fig. 6. The trajectory of sequence MH_01_easy.

TABLE IV
THE RMSE ERROR OF CAMERA POSE ESTIMATION RESULTS (UNIT: M).

Sequence	Our method	R-VIO	ROVIO	MSCKF	OKVIS
MH_01_easy	0.20	0.38	0.21	0.42	0.16
MH_02_easy	0.15	0.74	0.25	0.45	0.22
MH_03_medium	0.21	0.35	0.25	0.23	0.24
MH_04_difficult	0.31	1.03	0.49	0.37	0.34
MH_05_difficult	0.25	0.85	0.52	0.48	0.47
V1_01_easy	0.089	0.085	0.10	0.34	0.09
V1_02_medium	0.09	0.15	0.10	0.20	0.20
V1_03_difficult	0.15	0.13	0.14	0.67	0.24
V2_01_easy	0.092	0.080	0.12	0.10	0.13
V2_02_medium	0.13	0.16	0.14	0.16	0.16
Average error	0.1671	0.3955	0.232	0.342	0.225

RMSE results without loop detection are compared. The result of R-VIO comes from the original literature, and [26] presents the results of the other methods tested on the laptop. Their hardware platforms are better than ours, and compared results are listed in Table IV.

In this table, our method performs best on six of ten sequences compared with R-VIO and performs best on at least nine of ten sequences compared with the other methods. The difference to the best system on the other sequences is small. Our method also has the smallest average error (0.1671m for our, 0.3955m for R-VIO, 0.232m for ROVIO, 0.342m for MSCKF and 0.225m for OKVIS).

C. Time-consuming results

The time-consuming of our method is compared with the original VINS-Mono. Our method is integrated into the solveOdometry function in vins_estimator.cpp file, and other files are not modified. Therefore, it is enough to test the time

TABLE V
THE AVERAGE TIME-CONSUMING OF SOLVEODOMETRY FUNCTION FOR SOLVING ONE KEYFRAME (UNIT: MILLISECOND).

Sequence	Our method	VINS-Mono	Time difference
MH_01_easy	61.51	49.32	12.19
MH_02_easy	61.39	48.44	12.95
MH_03_medium	59.56	48.59	10.97
MH_04_difficult	57.32	48.72	9.12
MH_05_difficult	59.93	47.25	12.68
V1_01_easy	61.35	50.01	11.34
V1_02_medium	48.38	44.28	4.10
V1_03_difficult	40.74	37.09	3.65
V2_01_easy	56.78	48.03	8.75
V2_02_medium	55.03	42.22	12.81
Average time	56.20	46.39	9.81

difference of this function, which is more convenient and accurate than testing the whole system. We run five times in each sequence for every method and calculate the mean value as the final results. The average time-consuming of solveOdometry function to solve one keyframe is shown in Table V.

In this table, the time differences of sequences V1_02_medium, V1_03_difficult and V2_01_easy are smaller than the other sequences. Since bias calculating occupies most time of our algorithm, different map point number leads to different time-consuming. The texture of Vicon Room is simple than Machine Hall, and the camera rotation is faster than the other sequences in these small time difference sequences. Therefore, less map points are recovered, and the added time to solveOdometry function is little.

According to Table V, it can be seen that the average time-consuming of our method is larger 9.81ms than the VINS-Mono. This value is acceptable for practical applications.

VI. CONCLUSION

This paper proposes a camera pose correction method, which is compact and effective and reserves all system information. The relationship between the pose estimation error and the biased value of the map point is derived. Based on this relationship and the bias calculating method, the pose estimation results are corrected. We verify the effectiveness and efficiency of our method by comparing with other state-of-the-art algorithms. The future work will integrate our method

into other visual SLAM systems, which does not contain IMU information.

REFERENCES

- [1] H. Li, J. Yao, J. C. Bazin, *et al.*, “A Monocular SLAM System Leveraging Structural Regularity in Manhattan World”, IEEE International Conference on Robotics and Automation, pp. 2518-2525, 2018.
- [2] P. Kim, B. Coltin, and H. J. Kim, “Low-Drift Visual Odometry in Structured Environments by Decoupling Rotational and Translational Motion”, IEEE International Conference on Robotics and Automation, pp. 7247-7253, 2018.
- [3] V. Ovechkin and V. Indelman, “BAFS: Bundle Adjustment with Feature Scale Constraints for Enhanced Estimation Accuracy”, IEEE International Conference on Robotics and Automation, pp. 804-810, 2018.
- [4] M. Hsiao, E. Westman, and M. Kaess, “Dense Planar-Inertial SLAM with Structural Constraints”, IEEE International Conference on Robotics and Automation, pp. 6521-6528, 2018.
- [5] S. M. Nasiri, H. Moradi, and R. Hosseini, “A Linear Least Square Initialization Method for 3D Pose Graph Optimization Problem”, IEEE International Conference on Robotics and Automation, pp. 2474-2479, 2018.
- [6] C. Kerl, J. Sturm, and D. Cremers, “Dense Visual SLAM for RGB-D Cameras”, International Conference on Intelligent Robots and Systems, pp. 2100-2106, 2013.
- [7] Y. S. Shin, Y. S. Park, and A. Kim, “Direct Visual SLAM using Sparse Depth for Camera-LiDAR System”, IEEE International Conference on Robotics and Automation, pp. 5144-5151, 2018.
- [8] G. Grisetti, G. D. Tipaldi, C. Stachniss, and *et al.*, “Fast and accurate SLAM with RaoBlackwellized particle filters”, Robotics and Autonomous Systems vol. 55, no. 1, pp. 30-38, 2007.
- [9] C. Kim, R. Sakthivel, and W. K. Chung, “Unscented FastSLAM: A Robust and Efficient Solution to the SLAM Problem”, IEEE Transactions on Robotics vol. 24, no. 4, pp. 808-820, 2008.
- [10] C. Estrada, J. Neira, and J. D. Tardos, “Hierarchical SLAM: Real-Time Accurate Mapping of Large Environments”, IEEE Transactions on Robotics vol. 21, no. 4, pp. 588-596, 2005.
- [11] K. Tateno, F. Tombari, I. Laina, and *et al.*, “CNN-SLAM: Real-time dense monocular SLAM with learned depth prediction”, IEEE Conference on Computer Vision and Pattern Recognition, pp. 6243-6252, 2017.
- [12] J. L. Blanco, J. A. F. Madrigal, and J. Gonzalez, “Toward a Unified Bayesian Approach to Hybrid MetricTopological SLAM”, IEEE Transactions on Robotics vol. 24, no. 2, pp. 259-270, 2008.
- [13] H. Liu, M. Chen, G. Zhang, and *et al.*, “ICE-BA: Incremental, Consistent and Efficient Bundle Adjustment for Visual-Inertial SLAM”, IEEE Conference on Computer Vision and Pattern Recognition, pp. 1974-1982, 2017.
- [14] Y. Zhao and P. A. Vela, “Good Feature Selection for Least Squares Pose Optimization in VO/VSLAM”, International Conference on Intelligent Robots and Systems, pp. 1183-1189, 2018.
- [15] L. Han, L. Xu, D. Bobkov, and *et al.*, “Real-Time Global Registration for Globally Consistent RGB-D SLAM”, IEEE Transactions on Robotics vol. 35, no. 2, pp. 498-509, 2019.
- [16] J. Nikolic, J. Rehder, M. Burri, and *et al.*, “A Synchronized Visual-Inertial Sensor System with FPGA Pre-Processing for Accurate Real-Time SLAM”, IEEE International Conference on Robotics and Automation, pp. 431-437, 2014.
- [17] S. Leutenegger, P. Furgale, V. Rabaud, and *et al.*, “Keyframe-Based Visual-Inertial SLAM Using Nonlinear Optimization”, Robotics: Science and Systems, DOI: 10.1177/0278364914554813.
- [18] R. M. Artal and J. D. Tardos, “Visual-Inertial Monocular SLAM With Map Reuse”, IEEE Robotics and Automation Letter, vol. 2, no. 2, pp. 796-803, 2017.
- [19] R. M. Artal, J. M. M. Montiel, and J. D. Tardos, “ORB-SLAM: A Versatile and Accurate Monocular SLAM System”, IEEE Transactions on Robotics vol. 31, no. 5, pp. 1-17, 2015.
- [20] T. Qin, P. Lin, and S. Shen, “VINS-Mono: A Robust and Versatile Monocular Visual-Inertial State Estimator”, IEEE Transactions on Robotics vol. 34, no. 4, pp. 1004-1020, 2018.
- [21] C. Forster, M. Pizzoli, and D. Scaramuzza, “SVO: Fast Semi-Direct Monocular Visual Odometry”, IEEE International Conference on Robotics and Automation, pp. 15-22, 2014.
- [22] R. Hartley, “Multiple View Geometry in Computer Vision”, 2th edition, pp. 156.
- [23] M. Burri *et al.*, “The EuRoC micro aerial vehicle datasets”, International Journal of Robotics Research, vol. 35, no. 10, pp. 1157-1163, 2016.
- [24] H. Zheng and G. Huang, “Robocentric Visual-Inertial Odometry”, International Conference on Intelligent Robots and Systems, pp. 6319-6326, 2018.
- [25] M. Bloesch, S. Omari, M. Hutter, and R. Siegwart, “Robot Visual Inertial Odometry Using a Direct EKF-based Approach”, International Conference on Intelligent Robots and Systems, pp. 298-304, 2015.
- [26] J. Delmerico and D. Scaramuzza, “A Benchmark Comparison of Monocular Visual-Inertial Odometry Algorithms for Flying Robots”, IEEE International Conference on Robotics and Automation, pp. 2502-2509, 2018.
- [27] A. I. Mourikis and S. I. Roumeliotis, “A Multi-State Constraint Kalman Filter for Vision-Aided Inertial Navigation”, IEEE International Conference on Robotics and Automation, pp. 3565-3572, 2007.
- [28] S. Leutenegger, S. Lynen, M. Bosse, *et al.*, “Keyframe-Based Visual Inertial SLAM Using Nonlinear Optimization”, International Journal of Robotics Research, vol. 34, no. 3, pp. 314-334, 2015.
- [29] A. R. Chowdhury and R. Chellappa, “Statistical Error Propagation in 3D Modeling from Monocular Video”, IEEE Conference on Computer Vision and Pattern Recognition Workshop, 2003.